AIAA JOURNAL
Vol. 41, No. 8, August 2003

Curvature Effects in Burke–Schumann Spray Flame Extinction

J. B. Greenberg* and F. Grodek†
Technion—Israel Institute of Technology, 32000 Haifa, Israel

The effect of curvature on the extinction at the tip of laminar spray diffusion flames in coflow is analyzed. In particular, we look at the way spray-related parameters alter the tip curvature and what impact this influence has on flame-tip extinction. The spray is described using the sectional approach and is assumed to be quasi-monodisperse. The analysis reveals that the flame curvature is strongly changed by the droplet loading and the vaporization Damkohler parameter. It is found that the tip curvature decreases rather sharply for a certain range of values of the vaporization Damkohler number. The extent of the decrease increases with the initial droplet load. Under these circumstances flame extinction is inhibited. However, beyond this range flame extinction can actually be enhanced because of the presence of the droplets. This behavior, with its linkage to the flame-tip radius of curvature, is related to the manner in which the spray parameters dictate the shape and temperature of these spray flames.

Nomenclature

A_n	=	function defined in Eq. (8)
B	=	preexponential factor
b_F, b_O	=	functions used in extinction analysis, defined in Eqs. (16) and (17)
c	=	inner duct's half-width (normalized with respect to outer duct walls' half-width)
c_p	=	heat capacity
E	=	activation energy
G_n	=	quadratic function defined in Eq. (9)
H	=	Heaviside function
$m_{\text{totalfuel}}$	=	total initial fuel mass fraction (vapor and liquid)
Pe	=	Peclet number
Q	=	heat of reaction
R	=	outer duct's half-width
$\boldsymbol{R}$	=	universal gas constant
R^*	=	flame-tip radius of curvature
s_n	=	function defined in Eq. (7)
T	=	temperature (normalized by $c_p/Qm_{\text{totalfuel}}$)
T_a	=	activation energy parameter ($E/\boldsymbol{R}$)
T_v	=	temperature of onset of evaporation
T_0	=	temperature at $\eta = 0$
β, β_T	=	Schwab–Zeldovitch functions; Eq. (4)
β_g, β_d	=	components of solution, defined in Eqs. (6b) and (6c)
β_n	=	transformed Schwab–Zeldovitch functions; Eq. (A2)
Γ	=	normalized latent heat of vaporization
γ	=	mass fractions normalized with respect to total initial fuel mass fraction
Δ	=	vaporization Damkohler number
δ	=	ratio of mass fraction of liquid fuel to that of total fuel at central duct exit, referred to as liquid fuel load
$\tilde{\delta}$	=	parameter in extinction analysis; Eq. (15)
$\tilde{\delta}_{\text{ext}}$	=	Linan's extinction function; Eq. (13)
ε	=	small parameter; Eq. (18)
ν	=	stoichiometric coefficient
ξ, η	=	transverse and axial coordinates, respectively

Subscripts

d	=	liquid fuel
F	=	gaseous fuel
fl	=	flame front
O	=	oxidant
0	=	outer duct's exit

Introduction

A POPULAR method for modeling turbulent flame structure is through the concept of laminar flamelets. The response of these flamelets to stretch effects can be highly significant, leading to repercussions that modify the overall turbulent flame behavior. In many combustion engineering applications the fuel (and sometimes the oxygen) is supplied as a spray of droplets. Thus, the extended modeling of turbulent spray flames needs to consider laminar spray flamelets and their behavior. Some initial efforts in this direction have already been made using computer simulations.[1] The effect of stretch in laminar diffusion quasi-monodisperse and polydisperse spray flames has been extensively studied, both analytically and numerically.[2–6] However, it appears that no work has yet been dedicated to examining curvature effects in spray diffusion flames. In the context of gas flames Im et al.[7] carried out a combined theoretical/experimental study of the influence of flame curvature on the extinction of the tip of a Burke–Schumann diffusion flame. They found that negative stretch, in the form of compressive flame curvature, promotes burning and thereby retards extinction.

Little experimental work has been carried out on laminar coflowing spray diffusion flames.[8,9] But the sparse visible evidence seems to indicate that, as with gas diffusion flames, some form of flame-tip "opening" occurs. This is usually associated with local extinction. Therefore, in the current paper we extend previous analyses of Burke–Schumann spray diffusion flames to examine the question of the effect of curvature on flame-tip extinction. What is primarily of interest is the way in which spray-related parameters influence the flame curvature and what sort of impact, if any, this has on the flame extinction.

Problem Description

We consider the basic Burke–Schumann spray flame configuration (see Fig. 1) in which fuel vapor and droplets flow in an inner duct and airflows in an outer duct. Under appropriate operating conditions, after diffusive mixing of the two streams, a steady laminar spray diffusion flame is maintained. A constant density model is taken, and the velocities in the inner and outer ducts are taken to be constant and equal, as per Burke–Schumann's original gas flame analysis. The effect of relaxing this latter assumption was examined by Khosid and Greenberg[10] and shown to be of quantitative rather than qualitative significance. It is assumed that the various transport

Presented as Paper 2002-0623 at the 40th Aerospace Sciences Meeting, Reno, NV, 14–17 January 2002; received 15 March 2002; revision received 3 April 2003; accepted for publication 12 April 2003.

*Lady Davis Professor of Aerospace Engineering. Senior Member AIAA.
†Graduate Student, Faculty of Aerospace Engineering.

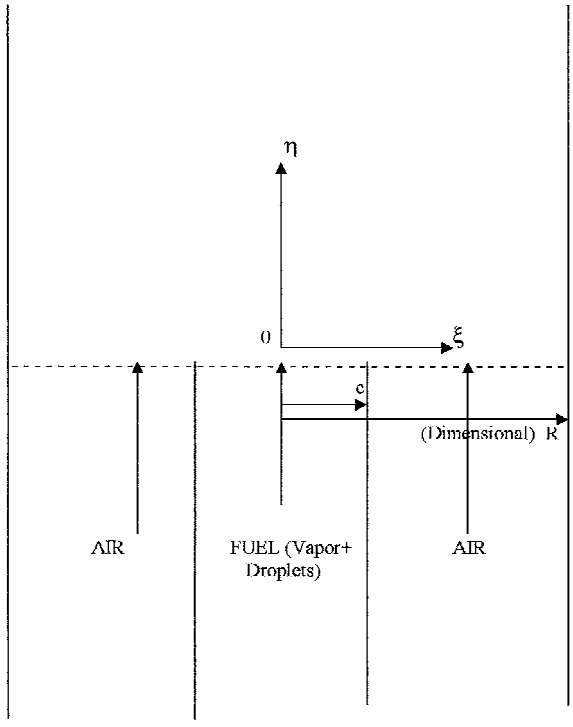

Fig. 1 Configuration for formation of Burke–Schumann spray diffusion flame.

coefficients such as thermal conductivity, diffusion coefficients, specific heat at constant temperature, latent heat of vaporization of the liquid droplets, etc. can be satisfactorily specified by representative constant values. Furthermore, the transport properties will be supposed to be determined primarily by the properties of the gaseous species. This follows from the implicit assumption that the liquid fuel volume fraction is sufficiently small. In addition, the Lewis numbers of the reactants (and products) are supposed to be unity. An overall reaction of the form

$$\text{Fuel} + \nu\text{Oxidant} \rightarrow \text{Products}$$

is taken to describe the chemistry, and we consider the fast chemistry limit. Under these circumstances we develop the leading-order outer solutions (for large chemical Damkohler number) and then consider extinction by looking at the inner structure of the flame.

The droplets are viewed from a far-field vantage point, that is, their average velocity is equal to that of their host environment. The actual description of the spray is based on the sectional approach.[11] In this method the pointwise size distribution of droplets in the spray is subdivided into a finite number of size sections, each of which contains droplets of diameters that fall within a certain size bracket. The mass balance of droplets in section j accounts for 1) the influx of droplets from section $j+1$, which have diminished in size and have thus become eligible for membership in section j, and 2) mass loss as a result of evaporation of droplets in section j. Sectional mass conservation equations can then be rigorously derived for the droplets in each size section. Here, for the sake of simplicity at the current stage, we take the spray to be quasi-monodisperse. An arbitrary polydisperse spray can also be treated at the expense of algebraic complexity. The temperature of the droplets is taken as equal to that of the surroundings; essentially the droplets heat-up time is small compared to the characteristic time associated with their motion. Droplet evaporation is assumed negligible until a prescribed reference temperature T_v (such as the boiling temperature of the liquid fuel) is attained.

The governing equations, written in terms of nondimensional quantities, are

$$Pe\frac{\partial\beta}{\partial\eta} = \frac{\partial^2\beta}{\partial\xi^2} + \frac{\partial^2\beta}{\partial\eta^2} + \Delta\gamma_d H(c-\xi) \tag{1}$$

$$Pe\frac{\partial\beta_T}{\partial\eta} = \frac{\partial^2\beta_T}{\partial\xi^2} + \frac{\partial^2\beta_T}{\partial\eta^2} - \Gamma\Delta\gamma_d H(c-\xi) \tag{2}$$

$$Pe\frac{\partial\gamma_d}{\partial\eta} = -\Delta\gamma_d \tag{3}$$

In these equations the Schwab–Zeldovitch functions β and β_T are defined by

$$(\beta, \beta_T) = (\gamma_F - \gamma_O, \gamma_O + T) \tag{4}$$

As usual, the stoichiometric coefficient is also incorporated in the denominator when normalizing the oxygen mass fraction. Large values of the vaporization Damkohler number represent a highly volatile fuel and/or small droplets in the spray. Conversely, small values correspond to a nonvolatile fuel and/or large droplets.[12] Δ is actually a complicated function of initial droplet diameters, the temperature differential between the droplets and the surrounding gas and the diffusivity and other properties of the fuel and its surroundings. This renders an analytical solution of the problem at hand unfeasible. So, while bearing in mind the restrictive nature of such a step, Δ is taken as constant for mathematical tractability. Despite this pragmatic reason for using a constant vaporization Damkohler number, there is some further justification to be found in the use of the d^2 law for a description of the vaporization coefficient. Reasonably accurate estimates of droplet size and vaporization time do provide some evidence of the validity of this law even under transient temperature conditions.[13–15] Labowsky[15] showed that the d^2 law predicts the actual vaporization history of an interacting droplet, especially in the initial period of combustion. Studies by Annamalai and Ryan[16] and Elperin and Krasitov[17] (the latter for random clusters of droplets) add further weight to Labowsky's findings. Adopting this law in the quasi-monodisperse sectional model of the spray then leads to a constant averaged value of the vaporization coefficient and, hence, of the vaporization Damkohler number. Finally, we quote the excellent agreement of theoretical predictions (based on the use of a constant value of Δ) with experimental measurements[9] as further support for our simplification.

Equation (3) is valid for the region $0 \le \xi \le c$, $\eta \ge 0$, where c is the normalized distance of the inner duct wall from the origin; elsewhere γ_d is identically zero. This expresses the fact that droplets are to be found only in the region above the inner duct because, in this model, there is no mechanism by means of which they can be diverted transversely.

The governing equations implicitly account for the different possible scenarios that are physically viable and that have been experimentally observed, namely, complete evaporation of the droplets before reaching the homogeneous diffusion flame front or prehomogeneous flame-front evaporation followed by posthomogeneous diffusion-flame burning of individual (or clusters of) droplets that survive the main flame front. That both of these possibilities are encaptured is readily discernible from the governing equations. First, Eq. (3) applies at all downstream stations, that is, for all $\eta > 0$, so that there is no restriction on the rate of vaporization, the latter being expressed via the specified value of the vaporization Damkohler number. Second, Eq. (1) for the Schwab–Zeldovitch function β also reveals the comprehensive nature of the model. In the region where no oxygen is present, β is positive by definition, and the source term on the right-hand side relates to the production of fuel vapor caused by the evaporation of droplets in the spray in the preflame zone. However, when β is negative the equation describes the behavior of the normalized mass fraction of oxygen, and the spray source term is still applicable, but now downstream of the homogeneous flame front (within the lateral bounds set by the Heaviside function). Here it serves as a sink that removes oxygen at a rate dictated by the rate of vaporization of the droplets. This corresponds to the postflame individual droplet-burning situation. Which scenario is under consideration will be strongly dependent on the value of the vaporization Damkohler number.

Because of the unity Lewis-number assumption, the chemical source term does not feature in Eqs. (1) and (2), but for later reference, in the context of flame extinction, we give its form as

$B\gamma_F\gamma_O \exp(-T_a/T)$ for the single-step global chemical reaction that describes the diffusion flame chemistry.

The boundary conditions are

$$\eta = 0, \qquad 0 \le \xi \le c: \qquad \beta - \frac{1}{Pe}\frac{\partial\beta}{\partial\eta} = 1 - \delta$$

$$\beta_T - \frac{1}{Pe}\frac{\partial\beta_T}{\partial\eta} = T_0, \qquad \gamma_d = \delta$$

$$\eta = 0, \qquad c \le \xi \le 1: \qquad \beta - \frac{1}{Pe}\frac{\partial\beta}{\partial\eta} = -\gamma_{O0}$$

$$\beta_T - \frac{1}{Pe}\frac{\partial\beta_T}{\partial\eta} = T_0, \qquad \gamma_d = 0$$

$$\eta > 0, \qquad \xi = 0, 1: \qquad \frac{\partial\beta}{\partial\xi} = \frac{\partial\beta_T}{\partial\xi} = 0$$

$$\eta \to \infty, \quad 0 \le \xi \le 1: \qquad \frac{\partial\beta}{\partial\eta}, \qquad \frac{\partial\beta_T}{\partial\eta} \to 0$$

The first two initial conditions imply a specified mass fractional/energy flux at the entrance to the duct in which combustion occurs. These conditions correctly account for the fact that it is possible for a buildup of fuel vapor to occur as a result of droplet evaporation so that a backflux of fuel vapor towards the entrance is experienced. (For this reason it can be shown that specification of the value of the Schwab–Zeldovitch functions themselves at the entrance, rather than the fluxes, leads to the incorrect limiting behavior of the solutions as the vaporization Damkohler number is allowed to tend to infinity.) As mentioned earlier, the onset of appreciable vaporization occurs when the temperature is equal to T_v. For ease of development, we take the temperature implied by the second boundary condition to be $T_0 \ge T_v$. The third set of conditions specifies the symmetry at $\xi = 0$, and the fact that the outer duct's walls are impervious to heat and mass transfer. The last conditions specify a state of far downstream equilibrium.

Solution

The aforedescribed problem can be readily solved to yield

$$\gamma_d(\eta) = \delta e^{-(\Delta/Pe)\eta} \tag{5}$$

$$\beta(\xi,\eta) = c(1+\gamma_{O0}) - \gamma_{O0} + \frac{2}{\pi}\sum_{n=1}^{\infty} A_n \frac{\sin n\pi c \cos n\pi\xi e^{s_n\eta}}{n(1-s_n/Pe)}$$

$$- \delta\left[\frac{c\delta e^{-(\Delta/Pe)\eta}}{1+\Delta/(Pe)^2} + \frac{2}{\pi}\Delta\delta e^{-(\Delta/Pe)\eta}\sum_{n=1}^{\infty}\frac{\sin n\pi c\cos n\pi\xi}{nG_n(\Delta)}\right]$$

$$= \beta_g(\xi,\eta) + \beta_d(\xi,\eta) \tag{6a}$$

where

$$\beta_g(\xi,\eta) = c(1+\gamma_{O0}) - \gamma_{O0}$$

$$+ \frac{2}{\pi}\sum_{n=1}^{\infty}(1+\gamma_{O_0})\frac{\sin n\pi c\cos n\pi\xi e^{s_n\eta}}{n(1-s_n/Pe)} \tag{6b}$$

$$\beta_d(\xi,\eta) =$$

$$-\delta\left\{\begin{array}{l}\dfrac{c\delta e^{-(\Delta/Pe)\eta}}{1+\Delta/(Pe)^2} + \dfrac{2}{\pi}\Delta\delta e^{-(\Delta/Pe)\eta}\displaystyle\sum_{n=1}^{\infty}\frac{\sin n\pi c\cos n\pi\xi}{nG_n(\Delta)} + \\ \dfrac{2}{\pi}\displaystyle\sum_{n=1}^{\infty}\left[1 - \frac{\Delta\delta}{G_n(\Delta)}\left(1+\frac{\Delta}{(Pe)^2}\right)\right]\frac{\sin n\pi c\cos n\pi\xi e^{s_n\eta}}{n(1-s_n/Pe)}\end{array}\right\} \tag{6c}$$

$$s_n = \frac{Pe - \sqrt{(Pe)^2 + 4(n\pi)^2}}{2} \tag{7}$$

$$A_n = 1 - \delta + \gamma_{O0} + \frac{\Delta\delta}{G_n(\Delta)}\left[1 + \frac{\Delta}{(Pe)^2}\right] \tag{8}$$

$$G_n(\Delta) = \left(\frac{\Delta}{Pe}\right)^2 + \Delta - (n\pi)^2 \tag{9}$$

$$\beta_T(\xi,\eta) = T_0 + \gamma_{O0}(1-c) - \Gamma\delta c + \frac{c\Gamma\delta e^{-(\Delta/Pe)\eta}}{1+\Delta/(Pe)^2}$$

$$- \frac{2}{\pi}\sum_{n=1}^{\infty}\left\{\gamma_{O0} + \frac{\Gamma\Delta\delta}{G_n(\Delta)}\left[1+\frac{\Delta}{(Pe)^2}\right]\right\}\frac{\sin n\pi c\cos n\pi\xi e^{s_n\eta}}{n(1-s_n/Pe)}$$

$$+ \frac{2}{\pi}\Gamma\Delta\delta e^{-(\Delta/Pe)\eta}\sum_{n=1}^{\infty}\frac{\sin n\pi c\cos n\pi\xi}{nG_n(\Delta)} \tag{10}$$

In the flame-sheet limit the flame location can be extracted from Eq. (6a) by determining the values of (ξ,η) for which $\beta = 0$. In the current study we consider overventilated flames only so that the flame tip is located at $\xi = 0$, $\eta = \eta_{\mathrm{fl}}^*$. The flame temperature can be similarly derived from both β and β_T by noting [see Eq. (4)] that in the oxygen-free zone $T = \beta_T$, whereas in the fuel vapor-free zone $T = \beta + \beta_T$. We only consider flame sheets for which the flame-tip temperature is physically feasible for sustaining a steady-state homogeneous flame front.

The radius of curvature of the flame at its tip can be deduced from the solutions and is found to be

$$R^* = \left|\frac{\dfrac{c\delta(\Delta/Pe)e^{-(\Delta/Pe)\eta_{\mathrm{fl}}^*}}{1+\Delta/(Pe)^2} + \dfrac{2}{\pi}\displaystyle\sum_{n=1}^{\infty}A_n\frac{\sin n\pi c s_n e^{s_n\eta_{\mathrm{fl}}^*}}{n(1-s_n/Pe)} + \dfrac{2}{\pi}\dfrac{\Delta^2\delta}{Pe}e^{-(\Delta/Pe)\eta_{\mathrm{fl}}^*}\displaystyle\sum_{n=1}^{\infty}\frac{\sin n\pi c}{nG_n(\Delta)}}{\dfrac{2}{\pi}\displaystyle\sum_{n=1}^{\infty}A_n\frac{(n\pi)^2\sin n\pi c e^{s_n\eta_{\mathrm{fl}}^*}}{n(1-s_n/Pe)} - 2\Delta\delta e^{-(\Delta/Pe)\eta_{\mathrm{fl}}^*}\displaystyle\sum_{n=1}^{\infty}\frac{n\pi\sin n\pi c}{G_n(\Delta)}}\right| \tag{11}$$

A brief guide to developing these results is given in the Appendix.

If there are no droplets present in the central duct $\delta = 0$, the various expressions reduce to those for a purely gaseous diffusion flame. These are in consonance with the results of Im et al.,[7] but mildly generalize their analysis, which specifies the mass fractions and temperature at $\eta = 0$ as opposed to the mass fractional and heat fluxes that are dictated here.

Steady-State Results

We have used the aforedescribed solutions to investigate the influence of the spray parameters on the flame characteristics. In Fig. 2 we show a plot of the flame height as a function of the vaporization Damkohler number for various droplet loads. We take the total fuel mass fraction to be constant so that different values of δ correspond to different combinations of the initial liquid and vapor mass fractions. The spectrum of values of the vaporization Damkohler number can be split into three regimes according to the underlying physics. What we shall call regime 1 refers to low values of $\Delta \le 3$–6 approximately (corresponding to large droplets and/or a nonvolatile fuel) for which the flame height is primarily determined

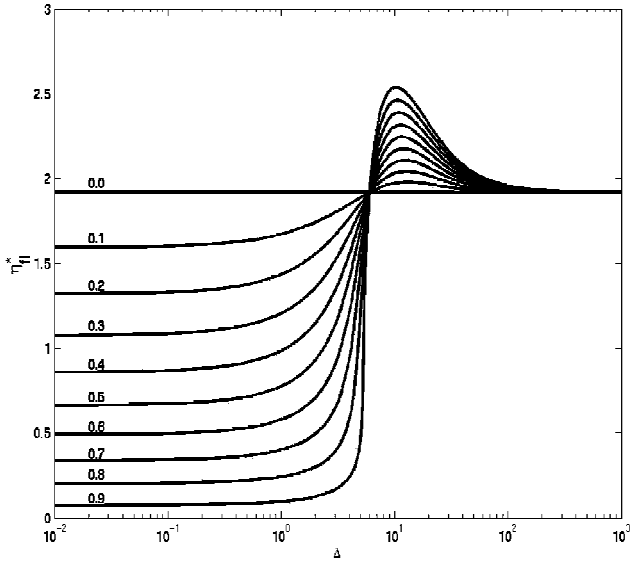

Fig. 2 Effect of vaporization Damkohler number on flame height for various initial droplet loads: $c = 0.166$, $\gamma_{O0} = 0.28$, $Pe = 10$.

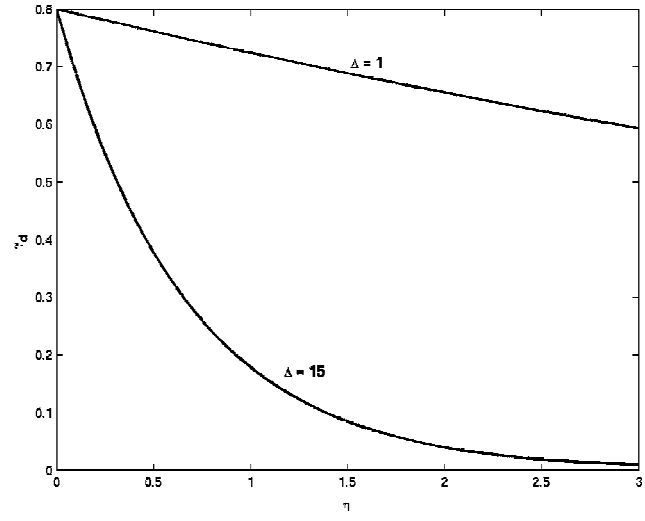

Fig. 3 Behavior of liquid fuel mass fraction with axial distance for two different vaporization Damkohler numbers: $\delta = 0.8$; other data as in Fig. 2.

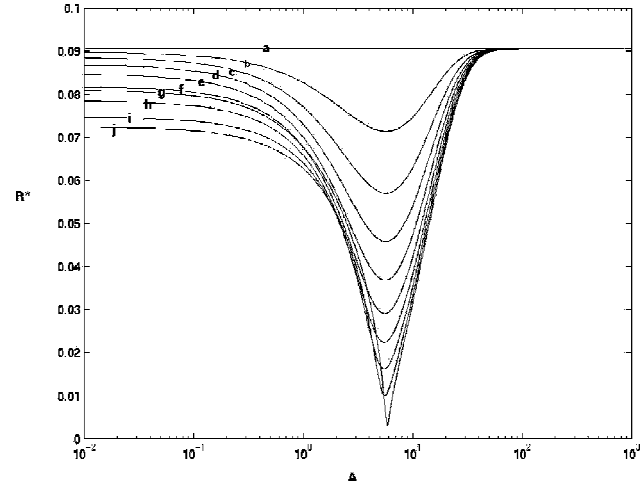

Fig. 4 Effect of vaporization Damkohler number on flame-tip curvature for various droplet loads: a–j corresponds to $\delta = 0$–0.9 in steps of 0.1; other data as in Fig. 2.

by the amount of fuel vapor initially present at the exit of the inner duct. The droplets vaporize slowly and supply little vapor to the homogeneous diffusion flame front. Subsequently, they traverse the flame front, become ignited as they pass through the flame into the hot oxygen-rich environment, and continue to burn downstream individually or in clusters in a heterogeneous mode of combustion.

For higher values of Δ, the droplets evaporate primarily upstream of the homogeneous diffusion flame front, so that the flame heights attained are greater than that of the classical gaseous diffusion flame ($\delta = 0$). This is regime 2. Finally, as $\Delta \to \infty$ (regime 3) complete evaporation of the droplets occurs close to $\eta = 0$, so that the classical Burke–Schumann diffusion flame height is reclaimed. {Parenthetically, we note the point of interest corresponding to $\Delta \approx 6$. Here the Burke–Schumann flame height is reattained apparently irrespective of the initial droplet load. Mathematically this point is understandable. The solution for $\beta(\xi, \eta)$ given in Eq. (6a) is split into two parts, namely, $\beta(\xi, \eta) = \beta_g(\xi, \eta) + \beta_d(\xi, \eta)$ [see Eqs. (6b) and (6c)], where $\beta_g(\xi, \eta)$ is the solution of Eq. (1) obtained when the nonhomogeneous spray term is omitted (i.e., the classical Burke–Schumann solution) and $\beta_d(\xi, \eta)$ is the particular integral. The flame height is found by determining the value of η for which $\beta(0, \eta) = 0$, that is, for which $\beta_g(0, \eta) + \beta_d(0, \eta) = 0$. Thus, when $\beta_g(0, \eta)$, $\beta_d(0, \eta) \neq 0$, then at the flame tip $\beta_g = -\beta_d$. In addition, it is also plausible that $\beta_d(0, \eta) = 0$, whence $\beta_g(0, \eta) = 0$, which will yield the classical Burke–Schumann flame height. Observing the expression for $\beta_d(0, \eta) = 0$ [see Eq. (6c)], it is readily seen that it is independent of δ. For c and Pe given, our calculations reveal that there is a single value of Δ for which $\beta_d(0, \eta) = 0$. Despite the fact that for this value of Δ all of the flames have an identical height, their shapes and tip temperatures (not shown here) are quite different from each other and from those of the classical Burke–Schumann gas flame. Such a situation is not entirely unfeasible physically, although a more general model that would require a full numerical solution of the governing equations including temperature and concentration-dependent transport and vaporization related coefficients is likely to lead to some spread around $\Delta = 6$. Nevertheless, the general classification of the three regimes should remain intact. In physical terms there is a rapid transition from predominantly homogeneous + heterogeneous combustion to primarily homogeneous combustion in the vicinity of $\Delta = 6$. As we shall see later, this transition expresses the subtle way in which the rate of vaporization and the flame shape are interconnected, with a subsequent profound effect on flame extinction.}

The aforementioned classification is verified in Fig. 3, where the profile of the liquid fuel mass fraction is shown as a function of the axial coordinate, for values of Δ equal to unity and 15, corresponding to two of the three physical regimes discussed earlier. It is evident that for $\Delta = 1$ the droplets continue to vaporize and burn beyond the flame front (located at $\eta \approx 0.27$), whereas for $\Delta = 15$ most of the fuel vapor is produced by the droplets prior to their reaching the flame front (located at $\eta \approx 2.1$).

In Fig. 4 the flame-tip curvature is plotted as a function of the vaporization Damkohler number for various droplet loads. For all droplet loads there exists a value of Δ for which the flame-tip's curvature reaches a minimum, and the minimum decreases with the droplet load. The behavior of the curves roughly reflects the aforementioned classification of flame height as a function of Δ and can be readily understood in terms of the shapes of the different flames, some of which are illustrated in Fig. 5. Now, in general, a tall flame will have a smaller tip radius of curvature than a shorter flame of about the same width. (Narrow and wide here are to be understood in terms of the distance to the η axis of the maximum protuberance of the flame front in the transverse direction.) Conversely, a wide flame will have a larger tip radius of curvature than a narrower flame having the same height. Referring to Fig. 5, we see that in regime 1, that is, for low values of Δ, the initial vapor load at $\eta = 0$ primarily determines the homogeneous flame shape. As Δ increases to a value of about six, more of the vaporized fuel becomes available before reaching the homogeneous flame front, but much of it is still consumed in postflame heterogeneous droplet

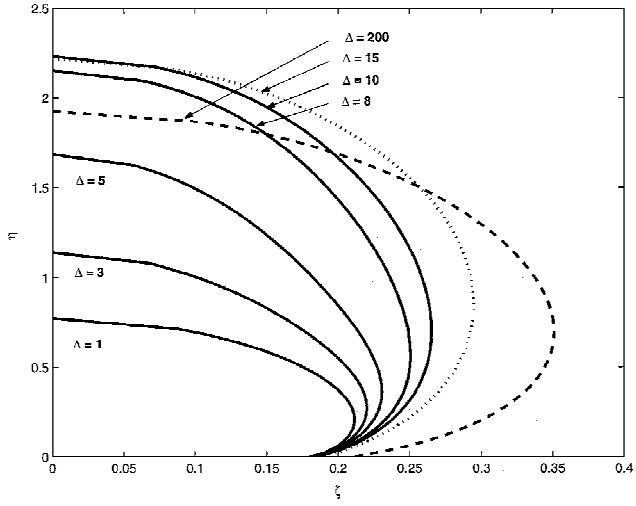

Fig. 5 Spray diffusion flame shapes for various values of the vaporization Damkohler number: $\delta = 0.5$; other data as in Fig. 2. Note that the flames having $\Delta = 1$ and 15 have identical tip radius of curvature.

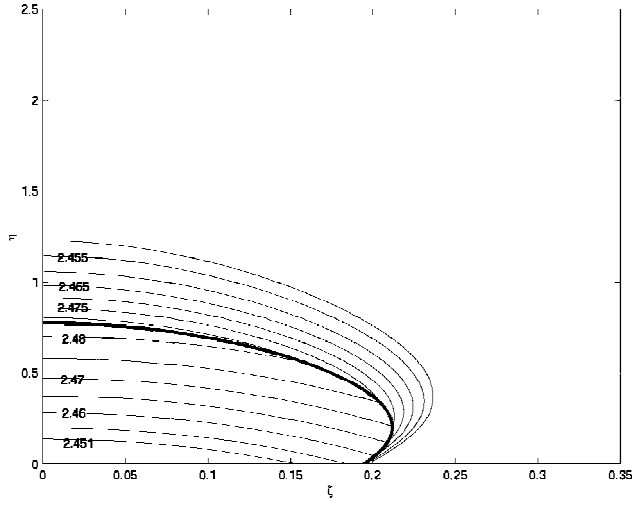

Fig. 6 Normalized flame temperature contours for the flame of Fig. 5 for which $\Delta = 1$.

combustion. The flames become taller but only slightly wider. Using Fig. 5, one can estimate that as Δ increases from 1 to 6 the flame height grows by about 153%, whereas the flame width increases by about 14%. Thus, under these circumstances it is understandable that the tip radius of curvature should decrease, as is seen in Fig. 4. Increasing Δ even further produces flames in regimes 2 and 3, for which most (if not all) of the fuel vapor produced by the droplets is devoured in the homogeneous flame front. Negligible or no post-flame heterogeneous droplet burning occurs now. Under these circumstances the flame heights (which increase and then decrease to that of the Burke–Schumann flame) vary within a relatively narrow band, whereas the flame width increases considerably. Again, estimating from Fig. 5, the flame heights vary by about 18%, whereas the width increases by about 46%. This leads to the increase in the radius of curvature observed in Fig. 4. Thus, we see that the behavior of the tip radius of curvature is strongly dictated by the flame shape. This, in turn, is dependent on whether the spray parameters imply a single homogeneous mode of combustion or a double homogeneous + heterogeneous mode. There exist two flames for any given value of the curvature. These flames correspond to different values of Δ. The shapes of two typical flames having the same droplet load and flame-tip curvature ($\sim$0.068) but different values of the vaporization Damkohler number ($\Delta = 1$ and 15) are included in Fig. 5. The difference between them is striking both in terms of their height and the extent to which they extend in the transverse

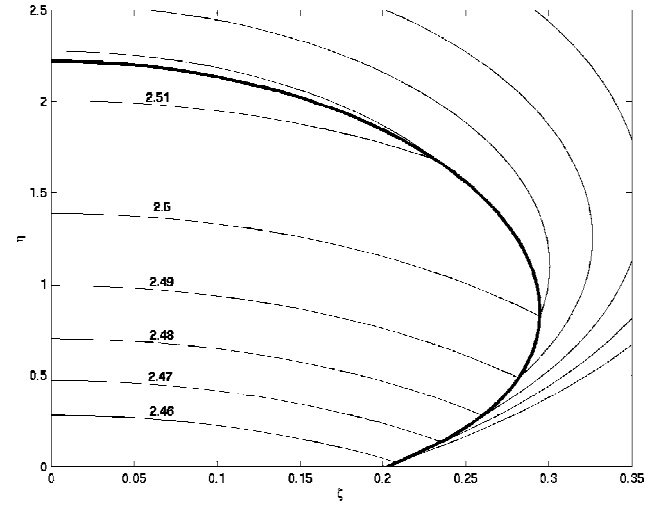

Fig. 7 Normalized flame temperature contours for the flame of Fig. 5 for which $\Delta = 15$.

direction. Their corresponding (normalized) temperature contours are shown in Figs. 6 and 7. A comparison clearly reveals the way in which the entire temperature field (including the flame tip temperature) is strongly influenced by the different operating conditions implied by the two considered values of Δ. Note that the flame for which $\Delta = 1$ is cooler than the flame for which $\Delta = 15$. This will be significant when we discuss flame-tip extinction.

Flame-Tip Extinction

Under the assumption that the homogeneous flame-front thickness is much smaller than the radius of curvature at the flame tip, a one-dimensional analysis of conditions for extinction can be carried out in the vicinity of $\xi = 0$, $\eta = \eta_{\mathrm{fl}}^*$. Use is made of the outer solutions already developed and follows the lines of Linan's[18] classical development of the inner structure of the diffusion flame. We simply quote the pertinent results here. It is found that for extinction to occur:

$$\tilde{\delta} \le \tilde{\delta}_{\mathrm{ext}} \tag{12}$$

where

$$\tilde{\delta}_{\mathrm{ext}} = e[(1-|\gamma|) - (1-|\gamma|)^2 + 0.26(1-|\gamma|)^3 + 0.055(1-|\gamma|)^4] \tag{13}$$

$$\gamma = \frac{b_F + b_O}{b_F - b_O} \tag{14}$$

$$\tilde{\delta} = \frac{4\varepsilon^3 B \exp(-T_f/T_a)}{(b_F - b_O)^2} \tag{15}$$

in which

$$b_F = \frac{(1-\Gamma)c\delta(\Delta/Pe)e^{-(\Delta/Pe)\eta_{\mathrm{fl}}^*}}{1+\Delta/(Pe)^2} + \frac{2}{\pi}\sum_{n=1}^{\infty}\frac{c_n s_n \sin n\pi c e^{s_n\eta_{\mathrm{fl}}^*}}{n(1-s_n/Pe)} + \frac{2}{\pi}\frac{\Delta^2}{Pe}\delta(1-\Gamma)e^{-(\Delta/Pe)\eta_{\mathrm{fl}}^*}\sum_{n=1}^{\infty}\frac{\sin n\pi c}{nG_n(\Delta)} \tag{16}$$

$$b_O = \frac{-\Gamma c\delta(\Delta/Pe)e^{-(\Delta/Pe)\eta_{\mathrm{fl}}^*}}{1+\Delta/(Pe)^2} - \frac{2}{\pi}\sum_{n=1}^{\infty}\frac{B_n s_n \sin n\pi c e^{s_n\eta_{\mathrm{fl}}^*}}{n(1-s_n/Pe)} - \frac{2}{\pi}\Gamma\delta\frac{\Delta^2}{Pe}e^{-(\Delta/Pe)\eta_{\mathrm{fl}}^*}\sum_{n=1}^{\infty}\frac{\sin n\pi c}{nG_n(\Delta)} \tag{17}$$

$$\varepsilon = \frac{T_{\mathrm{fl}}^2}{T_a} \tag{18}$$

Now an examination of Eq. (12) shows that, given the values of T_a and B, both $\tilde{\delta}$ and $\tilde{\delta}_{\text{ext}}$ depend on the four parameters Pe, γ_{O0}, δ, and Δ, the latter two characterizing the spray. Hence, upon specifying the values of any two of these parameters, a map can be constructed delineating the relevant operating conditions, defined by the other two parameters, which separate regions of flame extinction and existence. In addition, it can be shown that the factor $(b_F - b_O)^2$ in the denominator of Eq. (15) is proportional to the square of the radius of curvature [Eq. (11)]. Because it can be demonstrated that η^*_{fl}/Pe is approximately constant for large values of *Pe*, the implication is that smaller flame-tip radii of curvature inhibit extinction. Interestingly, this result carries through directly from the single gas-phase case[7] and is applicable irrespective of the droplet loading. In addition, referring to Fig. 4, it can be seen that the vaporization Damkohler number will play a critical role in determining the existence or extinction of the spray flames. The appearance of the minima in Fig. 4 is indicative of a range of values of Δ for which extinction can be inhibited.

In Fig. 8 the critical droplet load is plotted as a function of Δ for $Pe = 15$ and $\gamma_{O0} = 0.28$. Flame extinction/existence occurs for conditions above/below the curve, respectively. For values of Δ in regime 1, the lower flame temperatures make the flames particularly susceptible to extinction. Even a slight droplet load absorbs heat for vaporization (expressed mathematically via the parameter Γ), and this will cause extinction. In regime 2 the flames burn intensively, and their existence is not threatened by the endothermic droplet heat absorption. A large region exists in which no extinction occurs for any droplet load. Under such circumstances extinction is clearly inhibited. In regime 3 the flame temperatures become slightly lower, and the role of the droplet load reattains significance in determining whether extinction will occur or not.

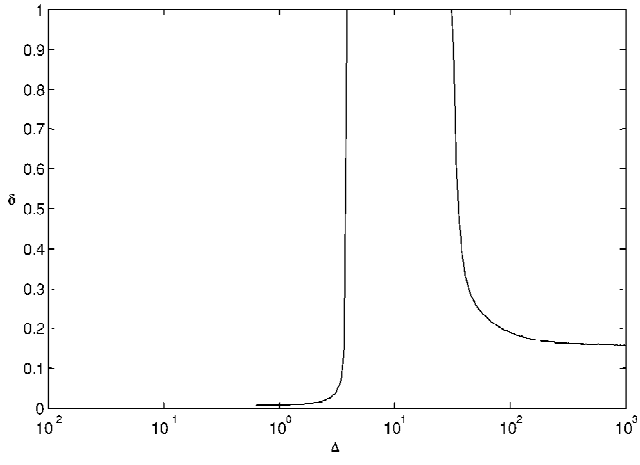

Fig. 8 Critical droplet loading as a function of vaporization Damkohler number: $Pe = 15$, $T_a = 61.6$, $B = 1.5 \times 10^{10}$, $\gamma_{O0} = 0.28$, and $\Gamma = 0.04$.

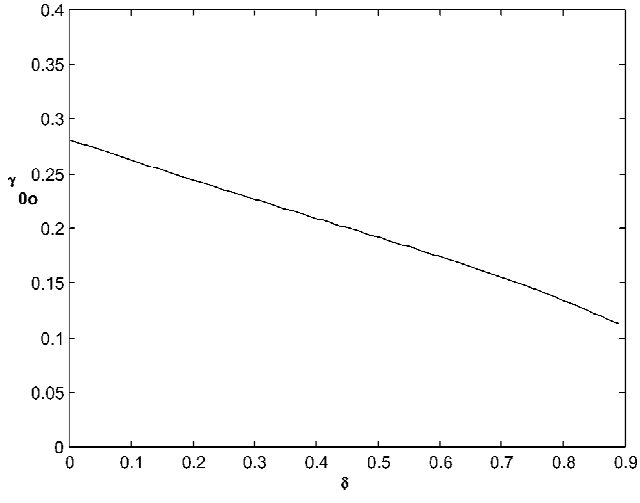

Fig. 9 Critical normalized oxygen mass fraction as a function of droplet loading: $\Delta = 1$; other relevant data as in Fig. 8.

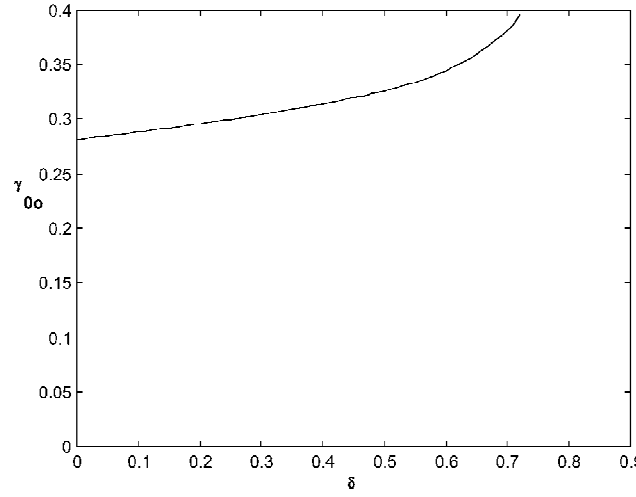

Fig. 10 Critical normalized oxygen mass fraction as a function of droplet loading: $\Delta = 10$; other relevant data as in Fig. 8.

In Figs. 9 and 10 $\gamma_{O0,\text{critical}}$ is drawn as a function of the droplet load for $Pe = 15$, and vaporization Damkohler numbers $\Delta = 1$ and 10, respectively. Flame extinction/existence occurs for conditions above/below the curves, respectively. It is observed that while the curve for $\Delta = 1$ decreases monotonically as the droplet load increases rather different behavior is seen for the higher value of Δ. This behavior can once again be explained in terms of the expression $(b_F - b_O)^2$, which appears in the denominator of Eq. (15). For the case of $\Delta = 1$, as the droplet load increases this factor increases, and the numerator of Eq. (15) decreases. The overall effect is therefore one of increasingly enhancing the region of operating conditions for extinction. However, for the case of $\Delta = 10$ the role of the reduced radius of curvature [which decreases as the droplet load increases, see Eq. (11)] is called into play, leading to a region in which flame extinction is inhibited and which grows in size as the droplet load increases.

Conclusions

We have shown that the extinction of the flame-tip radius in Burke–Schumann spray diffusion flames is strongly affected by the spray parameters (droplet load and vaporization Damkohler number). The shape of the flames in terms of their height and width plays a key role. In the current context these characteristics are strongly determined by the spray parameters. The analysis reveals that the flame-tip radius of curvature decreases rather sharply for a certain range of values of the vaporization Damkohler number. The extent of the decrease increases with the initial droplet load. Under these circumstances flame extinction is inhibited. However, beyond this range flame extinction can be enhanced because of the presence of the droplets. Roughly speaking, this behavior can be interpreted in terms of the flame shape and temperature. A smaller flame-tip radius implies a hotter, taller flame that is less susceptible to extinction. Larger values of the radius of curvature imply cooler, shorter flames that are more susceptible to extinction.

Appendix: Development of Outer Solutions

We give a brief outline of the development of the outer solutions. Integration of Eq. (3) to obtain the solution given in Eq. (5) is straightforward. Inserting this solution in Eqs. (1) gives

$$Pe\frac{\partial\beta}{\partial\eta} = \frac{\partial^2\beta}{\partial\xi^2} + \frac{\partial^2\beta}{\partial\eta^2} + \Delta\delta e^{-\Delta\xi}H(c-\xi) \qquad \text{(A1)}$$

Define the finite cosine transform of β according to

$$\beta_n(\eta) = \int_0^1 \beta(\xi, \eta) \cos n\pi\xi \, \mathrm{d}\xi, \qquad n = 0, 1, 2 \ldots \quad \text{(A2)}$$

Then multiplying Eq. (A1) and the boundary conditions by $\cos n\pi\xi$ and integrating between with respect to ξ between 0 and 1 yields

$$\frac{\mathrm{d}^2\beta_n}{\mathrm{d}\eta^2} - Pe\frac{\mathrm{d}\beta_n}{\mathrm{d}\eta} - (n\pi)^2\beta_n = -\frac{\Delta\delta}{n\pi}\sin n\pi c e^{-\Delta\eta}$$

$$n = 1, 2, 3 \ldots \quad \text{(A3)}$$

$$\frac{\mathrm{d}^2\beta_0}{\mathrm{d}\eta^2} - Pe\frac{\mathrm{d}\beta_0}{\mathrm{d}\eta} = -c\Delta\delta e^{-\Delta\eta}, \qquad n = 0 \quad \text{(A4)}$$

These equations can be readily solved using the transformed boundary conditions

$$\eta \to \infty: \qquad \frac{\mathrm{d}\beta_n}{\mathrm{d}\eta} \to 0 \quad \text{(A5)}$$

$$\eta = 0: \qquad \beta_n - \frac{1}{Pe}\frac{\mathrm{d}\beta_n}{\mathrm{d}\eta} = (1 - \delta + \gamma_{O0})\frac{\sin n\pi c}{n\pi}, \qquad n \neq 0 \quad \text{(A6)}$$

$$\beta_0 - \frac{1}{Pe}\frac{\mathrm{d}\beta_0}{\mathrm{d}\eta} = c(1 - \delta) - \gamma_{O0}(1 - c), \qquad n = 0 \quad \text{(A7)}$$

Inverting Eq. (A2) then produces the solution given in Eq. (6a). A similar procedure is necessary to extract β_T from Eq. (2).

The expression for the radius of curvature Eq. (11) is derived using the textbook formula

$$R^* = \left[1 + \left(\frac{\mathrm{d}\eta}{\mathrm{d}\xi}\right)^2\right]^{\frac{3}{2}} \Bigg/ \left|\frac{\mathrm{d}^2\eta}{\mathrm{d}\xi^2}\right| \quad \text{(A8)}$$

and is evaluated at the flame tip (having coordinates $\xi = 0$, $\eta = \eta_{\mathrm{fl}}^*$) The derivatives are obtained by differentiating the expression for $\beta(\xi, \eta)$ [Eq. (6a)] with respect to ξ and applying $\mathrm{d}\eta/\mathrm{d}\xi = 0$ at the flame tip.

Acknowledgments

J. Greenberg acknowledges the support of the Lady Davis Chair in Aerospace Engineering and the Technion Fund for the Promotion of Research. Thanks are also given Sharon Kislev for his dedicated technical assistance.

References

[1]Hollmann, C., and Gutheil, E., "Flamelet-Modeling of Turbulent Spray Diffusion Flames Based on a Laminar Spray Flame Library," *Combustion Science and Technology*, Vol. 135, 1998, pp. 175–192.

[2]Greenberg, J. B., and Sarig, N., "Coupled Evaporation and Transport Effects in Counterflow Spray Diffusion Flames," *Combustion Science and Technology*, Vol. 92, 1993, pp. 1–33.

[3]Continillo, G., and Sirignano, W. A., "Counterflow Spray Combustion Modeling," *Combustion and Flame*, Vol. 81, 1990, pp. 325–340.

[4]Dvorjetski, A., and Greenberg, J. B., "Influence of Non-Unity Lewis Numbers and Droplet Loading on the Extinction of Counter-Flow Spray Diffusion Flames," *Proceedings of the Combustion Institute*, Vol. 28, 2000, pp. 1047–1054.

[5]Li, S. C., Libby, P. A., and Williams, F. A., "Experimental and Theoretical Studies of Counterflow Spray Diffusion Flames," *Proceedings of the Combustion Institute*, Vol. 24, 1992, pp. 1503–1512.

[6]Massot, M., Kumar, M., Smooke, M. D., and Gomez, A., "Spray Counterflow Diffusion Flames of Heptane: Experiments and Computations with Detailed Kinetics and Transport," *Proceedings of the Combustion Institute*, Vol. 27, 1998, pp. 1975–1983.

[7]Im, H. G., Law, C. K., and Axelbaum, R. L., "Opening of the Burke–Schumann Flame Tip and the Effects of Curvature on Diffusion Flame Extinction," *Proceedings of the Combustion Institute*, Vol. 23, 1991, pp. 551–558.

[8]Chen, G., "An Experimental Investigation on Laminar Diffusion Flames of Monodisperse Fuel Sprays," Ph.D. Dissertation, Dept. of Mechanical Engineering, Yale Univ., Hartford, CT, May 1995.

[9]Golovanevsky, B., Levy, Y., Greenberg, J. B., and Matalon, M., "On Oscillatory Behavior of Laminar Spray Diffusion Flames: Theory and Experiment," *Combustion and Flame*, Vol. 117, Nos. 1–2, 1999, pp. 373–383.

[10]Khosid, S., and Greenberg, J. B., "The Burke–Schumann Spray Diffusion Flame in a Nonuniform Flowfield," *Combustion and Flame*, Vol. 118, 1999, pp. 13–24.

[11]Greenberg, J. B., Silverman, I., and Tambour, Y., "Stoichiometry and Polydisperse Effects in Premixed Spray Flames," *Combustion and Flame*, Vol. 93, 1993, pp. 97–118.

[12]Greenberg, J. B., and Cohen, R., "Dynamics of a Pulsating Spray-Diffusion Flame," *Journal of Engineering Mathematics*, Vol. 31, 1997, pp. 387–409.

[13]Law, C. K., and Sirignano, W. A., "Unsteady Droplet Combustion with Droplet Heating—II: Conduction Limit," *Combustion and Flame*, Vol. 28, 1977, pp. 175–186.

[14]Law, C. K., "Adiabatic Spray Vaporization with Droplet Temperature Transient," *Combustion Science and Technology*, Vol. 15, 1977, pp. 65–74.

[15]Labowsky, M., "Calculation of the Burning Rates of Interacting Fuel Droplets," *Combustion Science and Technology*, Vol. 22, 1980, pp. 217–226.

[16]Annamalai, K., and Ryan, W., "Interactive Processes in Gasification and Combustion. Part I: Liquid Drop Arrays and Clouds," *Progress in Energy Combustion Science*, Vol. 18, 1992, pp. 221–295.

[17]Elperin, T., and Krasitov, B., "Analysis of Evaporation and Combustion of Random Clusters of Droplets by a Modified Method of Expansion into Irreducible Multipoles," *Atomization and Sprays*, Vol. 4, 1994, pp. 79–97.

[18]Linan, A., "The Asymptotic Structure of Counterflow Diffusion Flames for Large Activation Energies," *Acta Astronautica*, Vol. 1, 1974, pp. 1007–1039.

J. R. Bellan
Associate Editor